Human Molecular Genetics, 2010, Vol. 19, No. 24 ***4759–4773***
doi:10.1093/hmg/ddq402
Advance Access published on September 21, 2010

The human deafness-associated connexin 30 T5M mutation causes mild hearing loss and reduces biochemical coupling among cochlear non-sensory cells in knock-in mice

Melanie Schütz[1], Pietro Scimemi[2,3], Paromita Majumder[4], Romolo Daniele De Siati[2,3], Giulia Crispino[4], Laura Rodriguez[4], Mario Bortolozzi[4,5,6], Rosamaria Santarelli[2,3], Anke Seydel[4], Stephan Sonntag[1], Neil Ingham[7], Karen P. Steel[7], Klaus Willecke[1,†] and Fabio Mammano[4,5,6,*,†]

[1]Institut fuer Genetik, Rheinische Friedrich-Wilhelms-Universitaet Bonn, Roemerstrasse 164, D-53117 Bonn, Germany, [2]Dipartimento di Specialità Medico Chirurgiche, Università di Padova, via Giustiniani 2, 35129 Padova, Italy, [3]Servizio di Audiologia, Ospedale 'Ca' Foncello', Treviso, Italy, [4]Istituto Veneto di Medicina Molecolare, Fondazione per la Ricerca Biomedica Avanzata, 35129 Padova, Italy, [5]Dipartimento di Fisica 'G. Galilei', Università di Padova, 35131 Padova, Italy, [6]Istituto CNR di Neuroscienze, Padova, Italy and [7]Wellcome Trust Sanger Institute, Wellcome Trust Genome Campus, Hinxton, Cambridge CB10 1SA, UK

Received June 15, 2010; Revised August 18, 2010; Accepted September 14, 2010

Mutations in the *GJB2* and *GJB6* genes, respectively, coding for connexin26 (Cx26) and connexin30 (Cx30) proteins, are the most common cause for prelingual non-syndromic deafness in humans. In the inner ear, Cx26 and Cx30 are expressed in different non-sensory cell types, where they largely co-localize and may form heteromeric gap junction channels. Here, we describe the generation and characterization of a mouse model for human bilateral middle/high-frequency hearing loss based on the substitution of an evolutionarily conserved threonine by a methionine residue at position 5 near the N-terminus of Cx30 (Cx30T5M). The mutation was inserted in the mouse genome by homologous recombination in mouse embryonic stem cells. Expression of the mutated Cx30T5M protein in these transgenic mice is under the control of the endogenous Cx30 promoter and was analysed via activation of the lacZ reporter gene. When probed by auditory brainstem recordings, $Cx30^{T5M/T5M}$ mice exhibited a mild, but significant increase in their hearing thresholds of about 15 dB at all frequencies. Immunolabelling with antibodies to Cx26 or Cx30 suggested normal location of these proteins in the adult inner ear, but western blot analysis showed significantly down-regulated the expression levels of Cx26 and Cx30. In the developing cochlea, electrical coupling, probed by dual patch-clamp recordings, was normal. However, transfer of the fluorescent tracer calcein between cochlear non-sensory cells was reduced, as was intercellular Ca^{2+} signalling due to spontaneous ATP release from connexin hemichannels. Our findings link hearing loss to decreased biochemical coupling due to the point-mutated Cx30 in mice.

INTRODUCTION

The genes encoding Cx26 (GJB2) and Cx30 (GJB6) are found within 50 kb of each other in the DFNB1 deafness locus on human chromosome 13. Non-sensory cells in the cochlea form intercellular networks coupled by gap junction channels composed primarily of Cx26 and Cx30 protein subunits (1),

*To whom correspondence should be addressed at: VIMM, Via G. Orus, 2, 35129, Padova, Italy. Tel: +39 0497922331; Fax +39 0497923260; Email: fabio.mammano@unipd.it
†The senior authors contributed equally to this publication.

which share 77% amino acid identity and appear to be coordinately regulated (2). Cx26 and Cx30 may assemble to form heteromeric and heterotypic intercellular channels (3) which allow the diffusional transfer of ions, metabolites and second messengers between cells (4–6). Of note, Cx26 is the only connexin whose structure has been resolved at atomic scale (7). In the cochlea, the *epithelial* gap junction network forms around embryonic day 16 (E16) and connects all supporting cells in the organ of Corti as well as adjacent epithelial cells (8) (a scheme of the cochlear duct is provided as Supplementary Material, Fig. S1). After the onset of hearing, which occurs in mice on postnatal day 12 (P12) (9), this network apparently subdivides further into two separate, medial and lateral, buffering compartments (10), which are thought to individually contribute to the homeostasis of sensory inner hair cells and outer hair cells (11). The *connective tissue* gap junction network starts to develop around birth and comprises interdental cells and fibrocytes in the spiral limbus, fibrocytes of the spiral ligament, basal and intermediate cells of the stria vascularis. The stria vascularis is responsible for exporting K^+ to the endolymph and generation of the endocochlear potential (12,13). The latter is an electrical potential difference between the endolymphatic and perilymphatic compartments of the cochlea, which appears around P5 and increases progressively to adult levels in excess of +80 mV by P18 (14). An early study demonstrated loss of endocochlear potential in a mutant guinea pig strain with an atrophic stria vascularis (15).

Mouse models lacking expression of Cx26 or Cx30 confirmed that these proteins are essential for hearing. Thus targeted ablation of Cx26 in the epithelial gap junction network of $Cx26^{OtogCre}$ mice (16) (obtained by crossing $Cx26^{loxP/loxP}$ mice with Otog-Cre mice expressing the Cre recombinase coding DNA under the control of the murine Otogelin promoter) ensued in cell death. This was accompanied by epithelial breaches shortly after the onset of hearing along with progressive and significant hearing loss ranging from 30 to 70 dB. The apoptotic process affected first the border and inner phalangeal cells that surround the inner hair cells and later extended to outer hair cells and to organ of Corti supporting cells around them. Inner hair cells were preserved in adult $Cx26^{OtogCre}$ mice, and cell death was not detected at any stage either in spiral ganglion neurons, in the fibrocytes of the spiral limbus and spiral ligament or in the stria vascularis. Endocochlear potential values developed normally up to P12–P13, thereafter decreased significantly in parallel with the appearance of epithelial breaches that compromised the integrity of the endolymphatic compartment. Additionally, K^+ concentration was also significantly lower in the endolymph of adult $Cx26^{OtogCre}$ mice compared with control animals.

Expression of the Cx26R75W dominant negative mutation in mice, obtained by injection into the pronucleus and random integration into the genome (17), resulted in deafness associated with significant histological abnormalities within the inner ear, including degeneration of the outer hair cells at 7 weeks of age. In a conditional Cx26 null mouse model (18) obtained by crossing $Cx26^{loxP/loxP}$ mice with Rosa26-Cre^{ERT} mice, in which Cre can be activated by a single injection, on E19, of the synthetic estrogen 4-hydroxytamoxifen, the earliest cell death occurred around P14 in outer hair cells and their surrounding supporting cells in the middle cochlear turn. Hence, death rapidly spread to the basal cochlear turn so that all types of cells had disappeared from the organ of Corti of these conditional Cx26 null mice a few months after birth. Unlike $Cx26^{OtogCre}$ mice, in these conditional Cx26 null mice, peripheral nerve fibres and the somata of spiral ganglion neurons at corresponding cochlear locations were completely degenerated as well, whereas hair cells in the apical cochlear turn were relatively preserved (18).

In $Cx30^{-/-}$ mice (19) (obtained by deletion of the Cx30 coding region), the cochleae were morphologically indistinguishable from those of $Cx30^{+/-}$ and wild-type mice up to P17. However, $Cx30^{-/-}$ mice failed to develop any measurable endocochlear potential, and adults had significantly decreased endolymphatic K^+ levels. Auditory thresholds increased from 84 dB on P17–18 to more than 100 dB in adult $Cx30^{-/-}$ mice, demonstrating that hearing impairment was more severe in $Cx30^{-/-}$ mice than in $Cx26^{OtogCre}$ mice. Correspondingly, the apoptotic process in $Cx30^{-/-}$ mice, albeit delayed by about 4 days relative to $Cx26^{OtogCre}$ mice, affected ultimately both inner hair cells and outer hair cells. Of note, transgenic expression of extra copies of the Cx26 gene from a modified bacterial artificial chromosome in a $Cx30^{-/-}$ background restored cochlea development and hearing (20).

In the original report (21), audiograms in Cx30T5M family members showed variable hearing impairment including a 20–50 dB decrease at frequencies of 2000–8000 Hz, a hearing threshold that increased over time above 500 Hz and a profound sensorineural deafness, thought to be hallmarks of dominant sensorineural deafness. In the paired oocyte assay, junctional currents were detected in *Xenopus laevis* oocytes expressing the wild-type Cx30 isoform. In contrast, no transjunctional conductance was present in oocytes expressing the Cx30 T5M mutant. Co-expressing wild-type and mutant Cx30 resulted in the inhibition of intercellular coupling, interpreted as a dominant-negative effect of the mutant connexin on wild-type Cx30.

Contrary to these results, other investigators reported normal electrical coupling in transfected human embryonic kidney cells (HEK293) overexpressing the mutant Cx30T5M protein, but impaired transfer of larger molecules such as propidium iodide or inositol 1,4,5-trisphosphate (IP_3) (22), a key intermediate implicated in the propagation of intercellular Ca^{2+} signals within connexin-expressing cells in the inner ear (23–26). Likewise, the Cx30T5M-mutated protein overexpressed in the human HeLa cell line showed correct targeting to the plasma membrane and yielded punctuated immunofluorescence signals similar to the wild-type protein, although the transfer of neurobiotin was impaired (27).

Here we report the insertion of the Cx30T5M mutation in the mouse genome. Our results show that this mutation interferes with hearing in mice, albeit less dramatically than in human patients, and link hearing loss to impaired biochemical coupling in the organ of Corti.

RESULTS

Generation of Cx30T5M mice

We generated Cx30T5M mutant mice via homologous recombination in murine HM1 embryonic stem cells (genetic

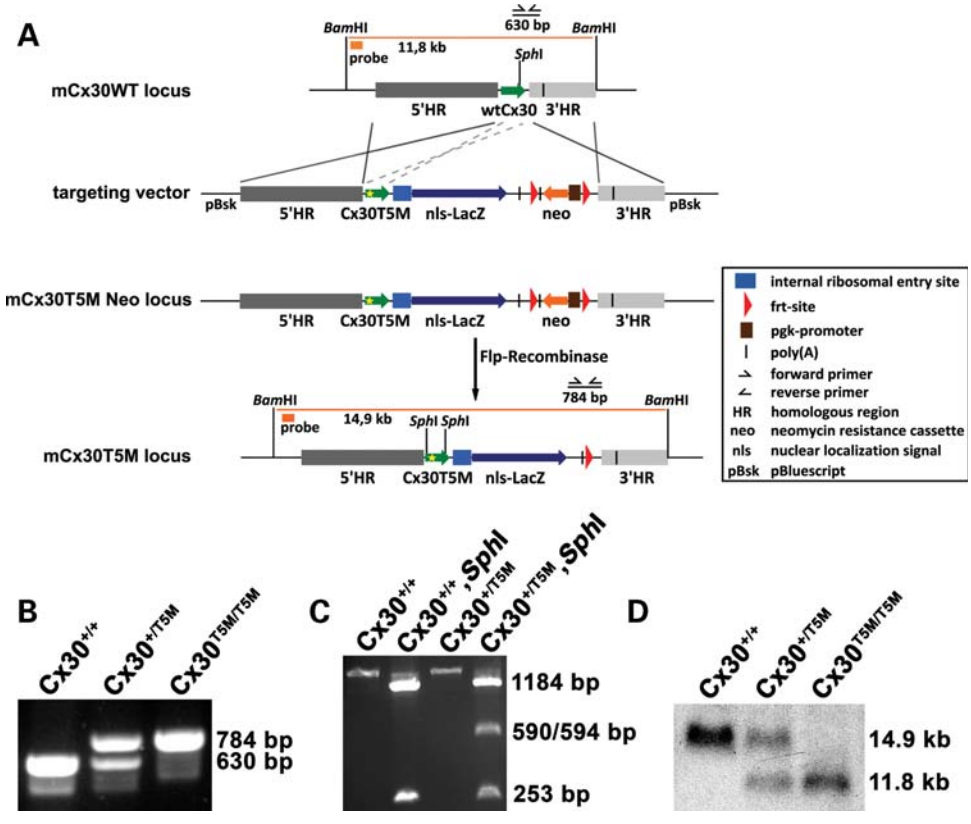

Figure 1. Generation of the Cx30T5M mice via homologous recombination. (**A**) Homologous recombination of the targeting vector into the genomic locus of Cx30 resulting in the mCx30T5M Neo locus. In mice, the neomycin resistance coding DNA is deleted by Flp recombinase activity resulting in the mCx30T5M locus. (**B**) PCR genotyping using the primers shown in (A). (**C**) PCR and subsequent digestion with *Sph*I to discriminate between wild-type and mutated Cx30 gene. (**D**) Southern blot hybridization indicating homologous recombination in mice.

background 129P2). The human point mutation T5M, which leads to a substitution of a threonine by a methionine residue at position 5 of the Cx30 protein, was inserted together with a *Sph*I restriction site via PCR mutagenesis into the corresponding mouse gene, *Gjb6* (Fig. 1A and B). The restriction site *Sph*I is specific for the mutated *Gjb6*, thus we could discriminate between mutated and wild-type *Gjb6* after PCR analysis and subsequent digestion with *Sph*I (Fig. 1C). To investigate the Cx30T5M expression *in vivo*, an internal ribosomal entry site (IRES) and the lacZ reporter coding DNA, with a nuclear localization signal (nls), were inserted after the Cx30T5M coding sequence. In order to select homologously recombined embryonic stem cell clones carrying the Cx30T5M construct, neomycin resistance coding DNA flanked by frt sites was cloned directly after the lacZ reporter DNA. Two out of 523 clones were identified to be homologously recombined and used for blastocyst injections. Matings of the resulting chimeras with C57BL/6 mice gave rise to heterozygous Cx30T5M mice. These mice were further interbred with deleter-Flp mice (28) to delete the neomycin resistance DNA and thus to avoid possible side effects of regulatory elements. Further breeding yielded homozygous Cx30T5M mice, which were viable, fertile and born at the expected Mendelian ratio (25%). The different genotypes were verified by PCR analyses and Southern blot hybridization (Fig. 1B and D).

Recording of auditory brainstem responses and measurement of endocochlear potential

Auditory brainstem responses are electrical signals evoked from the brainstem of a human or other mammal by the presentation of sound stimuli. To quantify hearing in Cx30T5M mice, we recorded auditory brainstem responses and, in particular, we assessed the IV wave thresholds for click and tone burst stimuli (8–14–20–26–32 kHz) in $Cx30^{+/+}$ ($n = 15$), $Cx30^{+/T5M}$ ($n = 23$) and $Cx30^{T5M/T5M}$ ($n = 16$) mice at several timepoints starting from P17 to P90 (see Supplementary Material, Fig. S2). Measurements at younger stages were not performed due to limitations intrinsic in the recording technique. Some mice were recorded three times (approximately P17, P35, P90) and showed no changes in hearing threshold against time. Thresholds determined by auditory brainstem responses were moderately (~15 dB) albeit significantly higher in $Cx30^{T5M/T5M}$ mice relative to $Cx30^{+/+}$ mice [$P < 0.005$, analysis of variance (ANOVA)], whereas we found no differences between $Cx30^{+/T5M}$ and $Cx30^{+/+}$ mice (Fig. 2A). This result is in contrast to the report that heterozygous human carriers of the Cx30T5M mutation are deaf (21). In keeping with the mild phenotype unveiled by auditory brainstem responses, measurements of endocochlear potential failed to reveal significant differences between $Cx30^{+/+}$, $Cx30^{+/T5M}$ and $Cx30^{T5M/T5M}$ mice. In contrast, endocochlear potential was

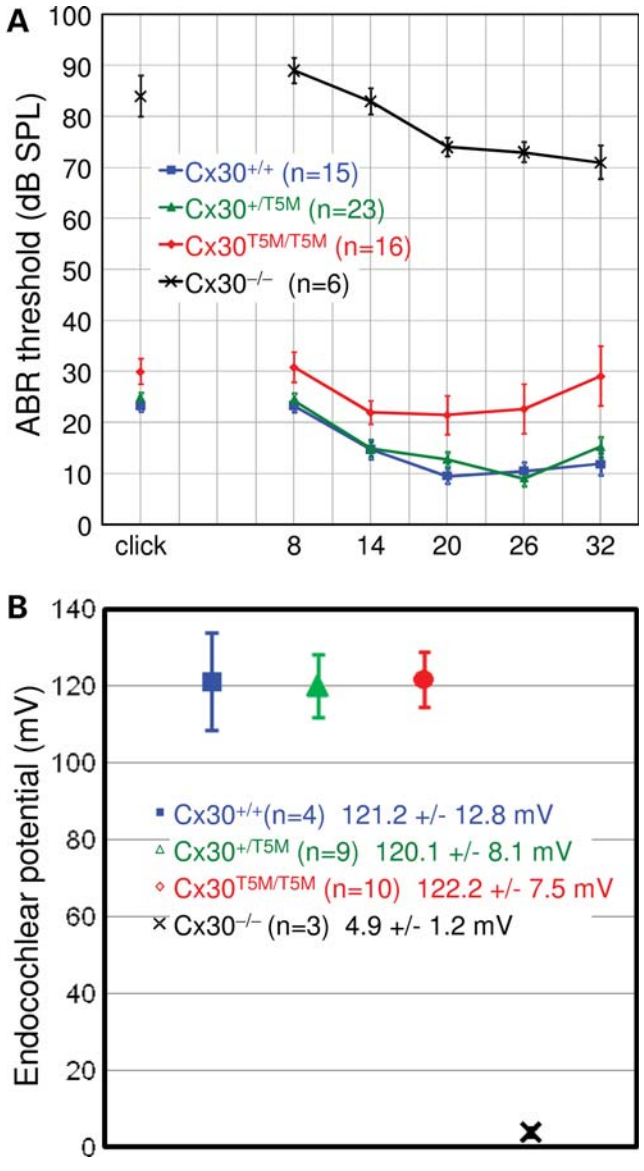

Figure 2. *In vivo* recordings from Cx30 mutant mice. (**A**) Audiograms for clicks and tone bursts for 8, 14, 20, 26 and 32 kHz obtained from auditory brainstem responses between P18 and P45. Bars represent the standard error. Compared with $Cx30^{+/+}$ controls, hearing threshold is mildly elevated only in $Cx30^{T5M/T5M}$ mice for all frequencies, but not in $Cx30^{+/T5M}$ mice; hearing loss is profound in $Cx30^{-/-}$ mice. (**B**) Endocochlear potential measurements obtained between P21 and P28 from Cx30T5M mutant mice and $Cx30^{-/-}$ mice.

dramatically reduced in $Cx30^{-/-}$ mice (Fig. 2B) that are profoundly deaf (Fig. 2A), in accord with previous reports (19,29).

Connexin immunolabelling in the adult cochlea

To characterize connexin expression in the transgenic mice, we performed immunolabelling with antibodies specific for Cx30 or Cx26 protein (Fig. 3). On P30, labelling patterns were similar, but not identical, for Cx26 and Cx30. No

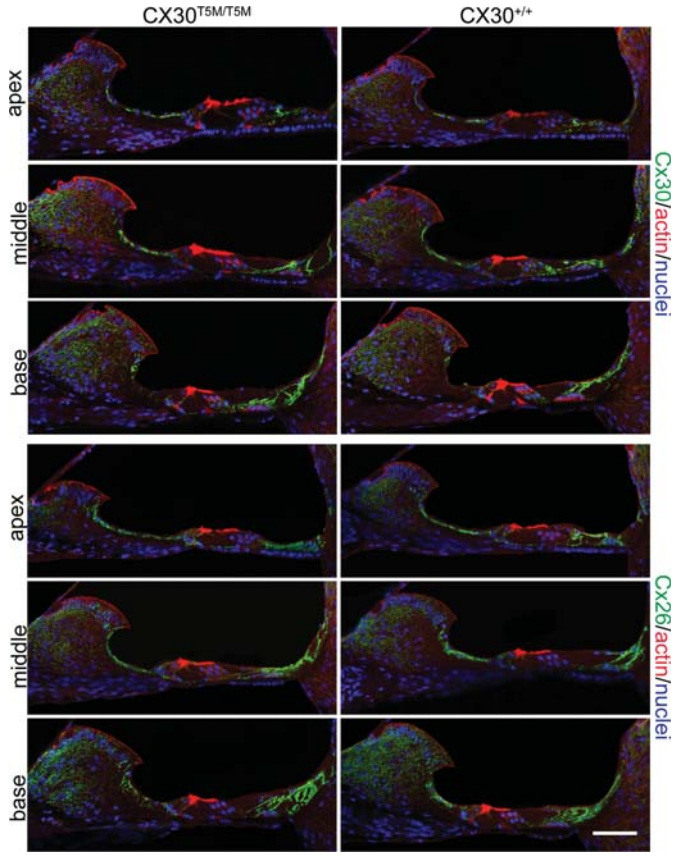

Figure 3. Connexin immunoreactity in the adult organ of Corti. Maximal projection rendering of two consecutive midmodiolar confocal optical sections, taken at 1 μm intervals in the indicated cochlear turns of $Cx30^{T5M/T5M}$ (left) and $Cx30^{+/+}$ mice (right) on P30. Cx30 and Cx26 expression was analysed with selective antibodies (green), nuclei were stained with DAPI (blue) and actin filaments with Texas red conjugated phalloidin (red). Scale bar, 50 μm.

discernible differences between $Cx30^{+/+}$, $Cx30^{+/T5M}$ and $Cx30^{T5M/T5M}$ mice were noticed.

Thus, in all three genotypes, Cx26 and Cx30 showed immunoreactivity in several sub-compartments of the cochlea at contact sites between supporting and epithelial cells of the organ of Corti on both sides of the hair cell region. Inner hair cells and outer hair cells showed no sign of immunoreactivity to Cx26 or Cx30 antibodies, in accord with the notion that sensory cells are not coupled by gap junction to any other cell type in the organ of Corti. Connexin immunoreactivity was evident in the spiral limbus, spiral ligament (Fig. 3), as well as basal and intermediate cells of the stria vascularis (see Supplementary Material, Figs S2 and S3). The latter finding is consistent with normal endocochlear potential levels measured in $Cx30^{+/T5M}$ and $Cx30^{T5M/T5M}$ mice indicated above (Fig. 2B).

Quantitative characterization of connexin expression in the adult cochlea by immunoblot analyses

To quantify connexin expression in the adult cochlea, on P30, we performed immunoblot analysis using antibodies specific for Cx30 or Cx26 (Fig. 4). The Cx30 protein level in

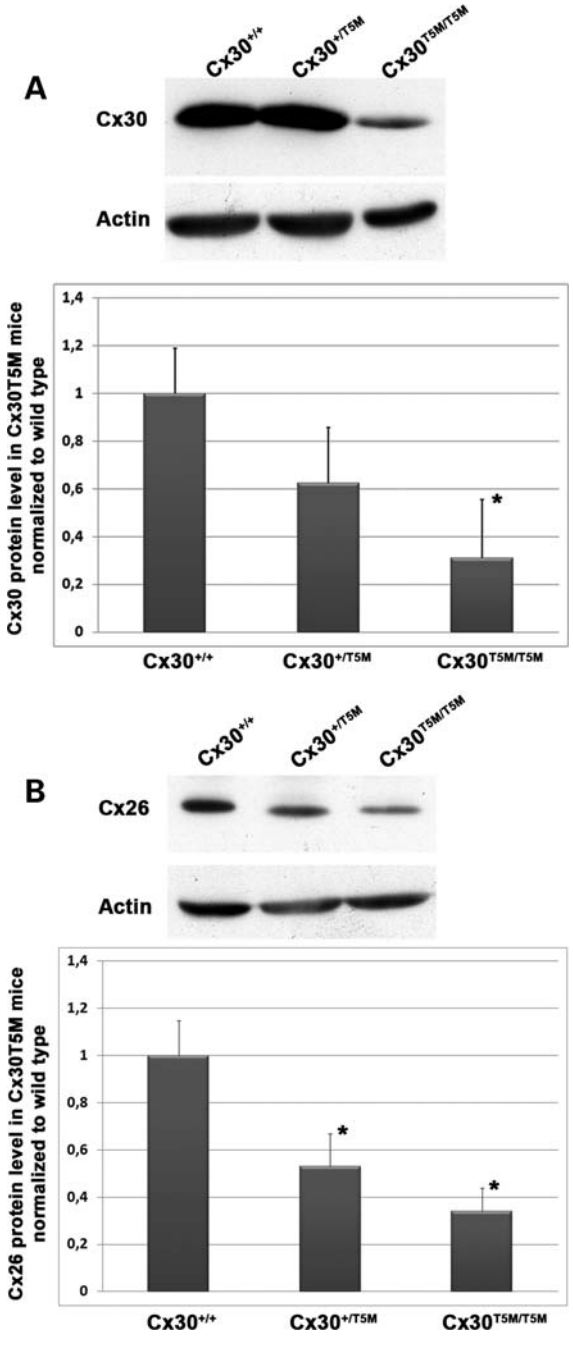

Figure 4. Quantitative immunoblot analyses of connexin expression in the adult cochlea. Protein levels were normalized to their corresponding actin bands for quantification. Asterisk in (**A**) indicates a significant reduction in Cx30 in $Cx30^{T5M/T5M}$ mice compared with Cx30 protein level in wild-type mice. Asterisks in (**B**) indicate a significant reduction in Cx26 in $Cx30^{T5M/T5M}$ mice compared with Cx26 protein level in wild-type mice.

$Cx30^{T5M/T5M}$ mice, normalized to the corresponding wild-type level (100%) was significantly decreased, on average, to 31 ± 25% ($P < 0.05$, $n = 3$). $Cx30^{+/T5M}$ mice expressed 63 ± 23% Cx30 protein ($n = 5$). The Cx26 protein level was significantly reduced to 53 ± 14% in adult $Cx30^{+/T5M}$ ($P < 0.05$, $n = 5$) and to 34 ± 14% in $Cx30^{T5M/T5M}$ mice ($P < 0.05$, $n = 3$). To estimate the significance of differences between genotypes, we used the independent two-sample, two-tailed test. The results of the immunoblot analyses were relatively variable, as indicated by the relatively large margin of error.

Characterization of gap junction channel permeability in the developing cochlea by fluorescence recovery after photobleaching

Functional gap junction channels are crucial for maturation of different tissues (30). In particular, Cx26 and Cx30 are essential for survival and development of the organ of Corti (16,19). Several lines of experiments indicate that permeability to larger metabolites, rather then small inorganic ions, may play an important role in the development, physiology and aetiology of connexin-related diseases (5). Furthermore, the effect of single point mutations can be subtle, discriminating between molecules having the same net charge but different charge distribution (5). In order to determine whether the mild hearing loss in $Cx30^{T5M/T5M}$ mice may be ascribed to a diminished cell–cell coupling during the crucial post-natal period, we performed fluorescence recovery after photobleaching assays (31) in cochlear cultures obtained from P5 mice (2,25,26). In particular, we focused on non-sensory cells of the receding greater epithelial ridge, the region of the epithelium that gives rise to the inner hair cells and medial non-sensory cells (32–34). We also investigated non-sensory cells in the lesser epithelial ridge, the area thought to give rise to the outer hair cells and lateral non-sensory cells (32–34) (Fig. 5A).

After overnight incubation *in vitro*, cochlear organotypic cultures were loaded with the acetoxymethyl (AM) ester of the fluorescent tracer calcein (MW 622, net charge −4) that diffuses through gap junction channels of non-sensory cells in cochlear organotypic cultures (2,25,26). Following the delivery of a 405 nm laser pulse to a restricted tissue area, the intracellular calcein fluorescence was partially restored via diffusion of the indicator dye through gap junction channels from adjacent unbleached cells in wild-type cultures (Fig. 5B, blue traces). Incomplete recovery of fluorescence intensity is ascribed to the fraction of the calcein pool which is not available for intercellular transfer (immobile fraction), due to trapping into subcellular organelles and/or binding to subcellular structures (35). These experiments clearly indicate that non-sensory cells in the developing cochlea of wild-type mice are dye-coupled in all cochlear turns. The different time courses of fluorescence traces in the lesser epithelial ridge (Fig. 5B, right) compared with the greater epithelial ridge (Fig. 5B, left) is indicative of a substantially larger immobile fraction in the latter. The Cx30T5M mutation caused a modest reduction of dye coupling levels in heterozygous cultures (Fig. 5B, green traces) but a substantial reduction in homozygous cultures (Fig. 5B, red traces). The process of fluorescence recovery after photobleaching was inhibited by pre-incubating cochlear cultures for 20 min in an extracellular medium (EXM, see Materials and Methods) supplemented with 100 μM carbenoxolone, a broad spectrum inhibitor of connexin channels (36) (Fig. 5B, black traces). The residual downward peak, which is resistant to carbenoxolone, is due to a small and rapid recovery of fluorescence caused by the diffusion of dye within the cell from deeper, relatively unbleached regions to more superficial, bleached regions.

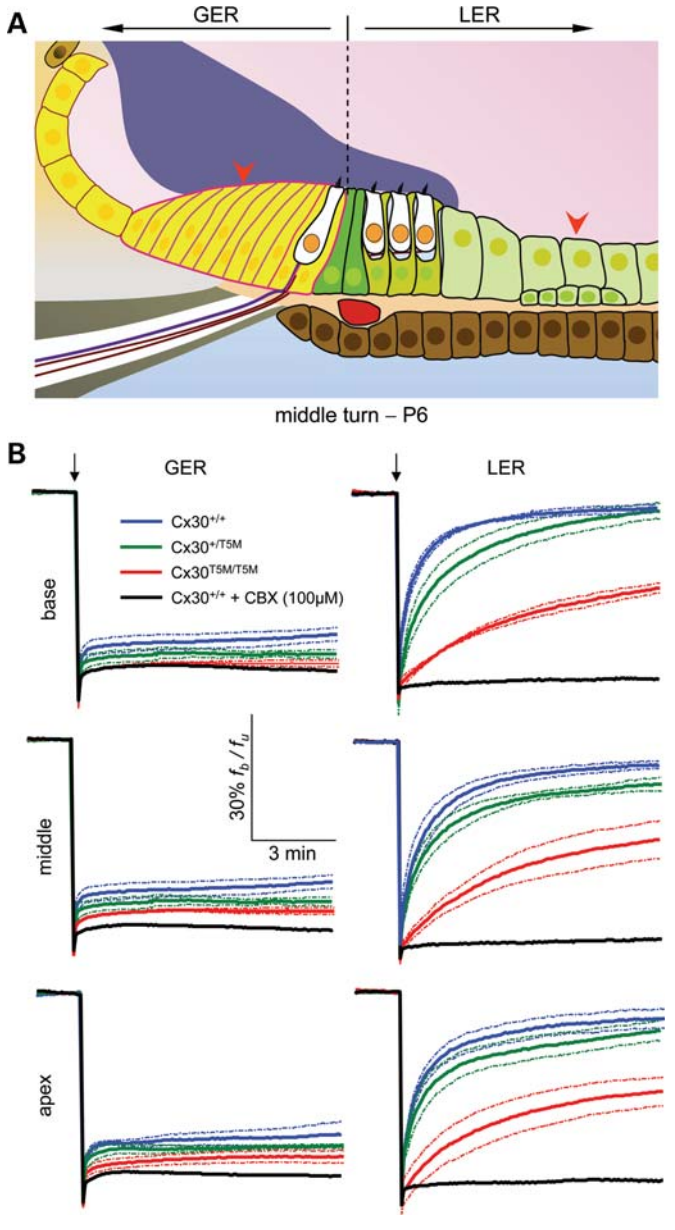

Figure 5. Dye coupling through gap junction channels in the developing cochlea. (**A**) Scheme of the sensory epithelium in the developing cochlea (middle turn, P6). Arrowheads indicate the approximate position of laser foci in the receding greater epithelial ridge (GER) and in the lesser epithelial ridge (LER). For comparison, see Supplementary Material, Figure S1. (**B**) Shown are plots of f_b/f_u (bleached over unbleached fluorescence intensity) versus time from the base, middle and apex of the cochlea (see Materials and Methods). Solid lines are averages of $n = 3$ independent experiments; dashed lines indicate 95% confidence intervals. Downward arrows mark the time of laser pulse delivery. CBX is a non-specific inhibitor of gap junction channels (36).

Measurement of electrical coupling in the developing cochlea

To quantify electrical coupling, we performed dual patch-clamp recordings from cell pairs of cochlear organotypic cultures obtained on P5 and tested after overnight incubation *in vitro*. Recent work demonstrated that, in this type of culture prepared from the basal cochlear turn, Cx26 and Cx30 form a network of gap junction plaques that interconnect uniformly all non-sensory cells of the lesser epithelial ridge (26), which was therefore used for these recordings. Junctional conductance, measured in an EXM, was similar in wild-type and homozygous cultures (5.7 ± 1.1 nS, $n = 4$ cultures from $Cx30^{+/+}$ mice; 5.9 ± 0.5 nS, $n = 3$ cultures from $Cx30^{T5M/T5M}$ mice; $P = 0.87$, ANOVA). These results, obtained in native tissues, are consistent with normal electrical coupling reported in transfected HEK293 cells overexpressing the mutant Cx30T5M protein (22).

Intercellular calcium signalling in cochlear non-sensory cells via ATP release through connexin hemichannels

Cochlear Cx26 and Cx30 also form unpaired connexons (37), i.e. non-junctional connexin *hemichannels* (38–41). Recent work highlighted the presence of hemichannels at a high density at the endolymphatic surface of the epithelium (26). Using cochlear organotypic cultures from mice with defective expression of pannexin 1, $P2X_7$ receptors, Cx30 or Cx26, previous work demonstrated that, in response to activation of a $P2Y/PLC/IP_3/Ca^{2+}$ signalling cascade, hemichannels formed by these connexins release ATP from the endolymphatic surface of cochlear non-sensory cells (25), whereas gap junction channels allow the concomitant diffusion of Ca^{2+} mobilizing second messengers from one cell to others coupled to it (23,25). Before the onset of hearing, non-sensory cells of the receding greater epithelial ridge spontaneously release ATP into the extracellular space; released ATP in turn activates purinergic receptors on cells in the neighbourhood of the release site, causing a rise in $[Ca^{2+}]_i$ (42,43).

We used the Ca^{2+} sensor fluo-4 to monitor spontaneous Ca^{2+} transient events in organotypic cultures of cochlear middle turns obtained from P5 mice and tested after overnight incubation *in vitro*. Spontaneous Ca^{2+} transients were readily detected from non-sensory cells of the greater epithelial ridge in wild-type organotypic cultures (Fig. 6A and Supplementary Material, Movie S1) bathed in ECM (see Materials and Methods), an EXM containing a reduced, endolymph-like $[Ca^{2+}]$ that favours hemichannel opening (25). The same release site generated multiple events during a typical recording session lasting a few minutes. Transients were detected also in the lesser epithelial ridge, mostly in Deiters' and Hensen's cells, but were not included in this analysis due to the lower frequency of occurrence. This spontaneous Ca^{2+} signalling activity was inhibited by flufenamic acid (50 μM), a known blocker of connexin hemichannels (25,44–48), and resumed after washout of the inhibitor. Results comparable to those shown in Figure 6A were obtained in two other cultures treated with flufenamic acid, as well as in one culture treated with niflumic acid (200 μM), which is also reported to block connexin hemichannels (25,46,47,49). Our proposed schematization of the molecular mechanisms underlying intercellular Ca^{2+} signalling in non-sensory cells of the developing cochlea via ATP release through connexin hemichannels is presented in Figure 6B.

To quantify spontaneous Ca^{2+} signalling activity, we collected data under uniform conditions from non-sensory cells of the receding greater epithelial ridge. In particular, we

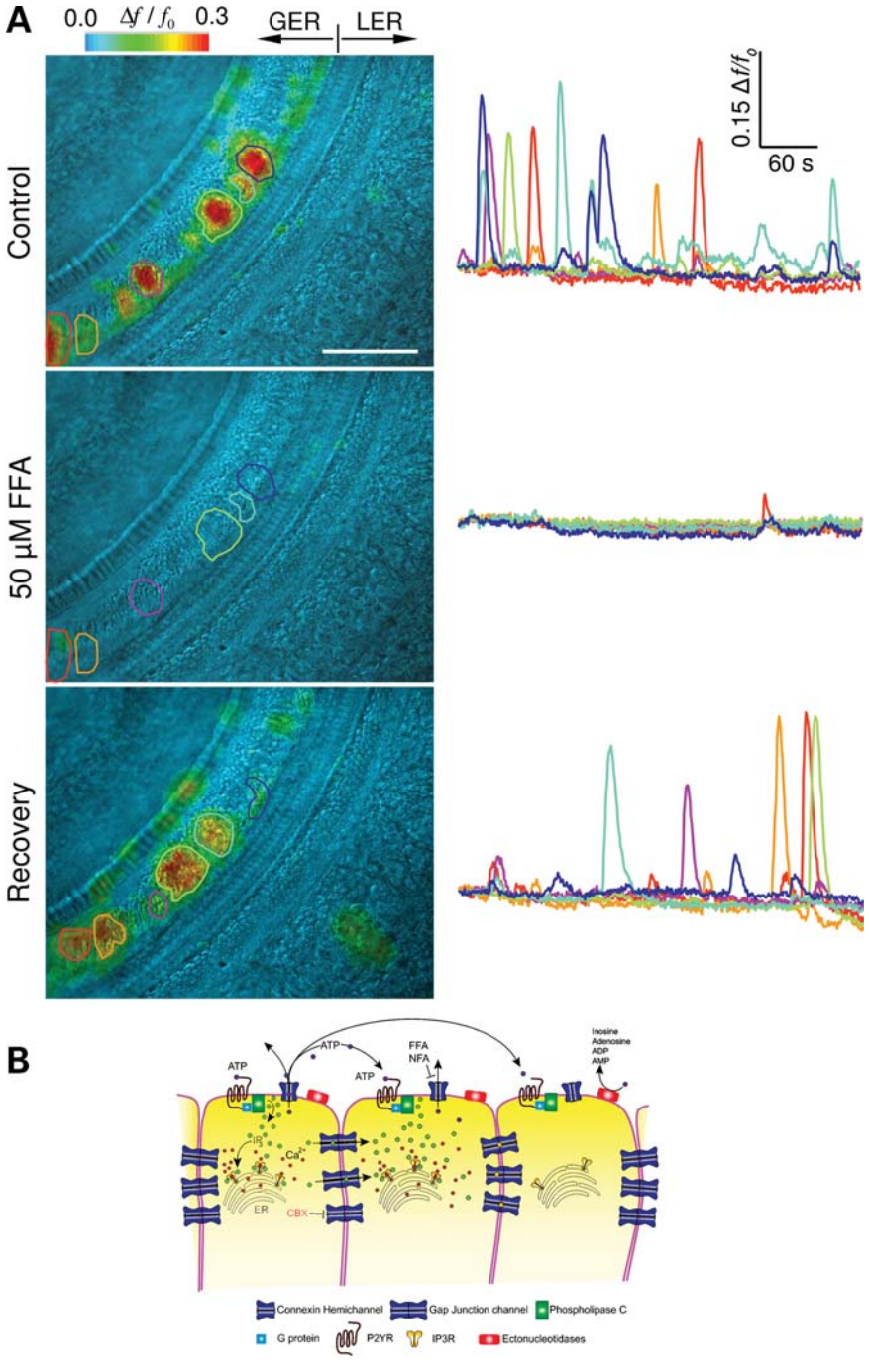

Figure 6. Spontaneous Ca^{2+} signalling activity in the developing cochlea is reversibly inhibited by the connexin hemichannel blocker flufenamic acid. (**A**) *Top* (left): False colour image of relative fluoresce changes, encoded as shown by the colour scale bar, obtained as a maximal projection rendering of all frames from a P5 cochlear culture loaded with the Ca^{2+} reporter fluo-4 and imaged for 7 min at 1 frame/s; six ROIs are shown superimposed on different Ca^{2+} hot spots; GER, greater epithelial ridge; LER, lesser epithelial ridge; scale bar, 100 μm. *Top* (right): Fluo-4 traces obtained as pixel averages from the six ROIs. *Middle*: Same as *Top* (including ROIs) following 20 min incubation with flufenamic acid (50 μM), a blocker of connexin hemichannels. *Bottom*: Recovery after washout of flufenamic acid; note different sets of six ROIs. (**B**) Scheme illustrating the molecular mechanisms underlying intercellular Ca^{2+} signalling in non-sensory cells of the developing cochlea via ATP release through connexin hemichannels. P2YR, P2Y receptors, is a family of G protein-coupled purinergic receptors stimulated by nucleotides such as ATP, ADP, UTP, UDP and UDP-glucose; IP_3R, inositol trisphosphate receptor, is a membrane glycoprotein complex acting as Ca^{2+} channel of the endoplasmic reticulum activated by IP_3. FFA, flufenamic acid; NFA, niflumic acid.

fixed illumination intensity, exposure time, frame rate and total duration of recording sessions (7 min). Pooled data are presented in Figure 7 and Table 1 ($n = 4$ cultures from four mice of each type). The area invaded by a single Ca^{2+} transient in cultures from $Cx30^{+/+}$ ($1.35 \pm 1.13 \times 10^3$ μm^2) and $Cx30^{T5M/T5M}$ mice ($1.22 \pm 1.06 \times 10^3$ μm^2) was similar (mean ± s.d.; $P = 0.83$, ANOVA). The area of apical plasmalemma of the tall columnar cells that fill the ridge at this

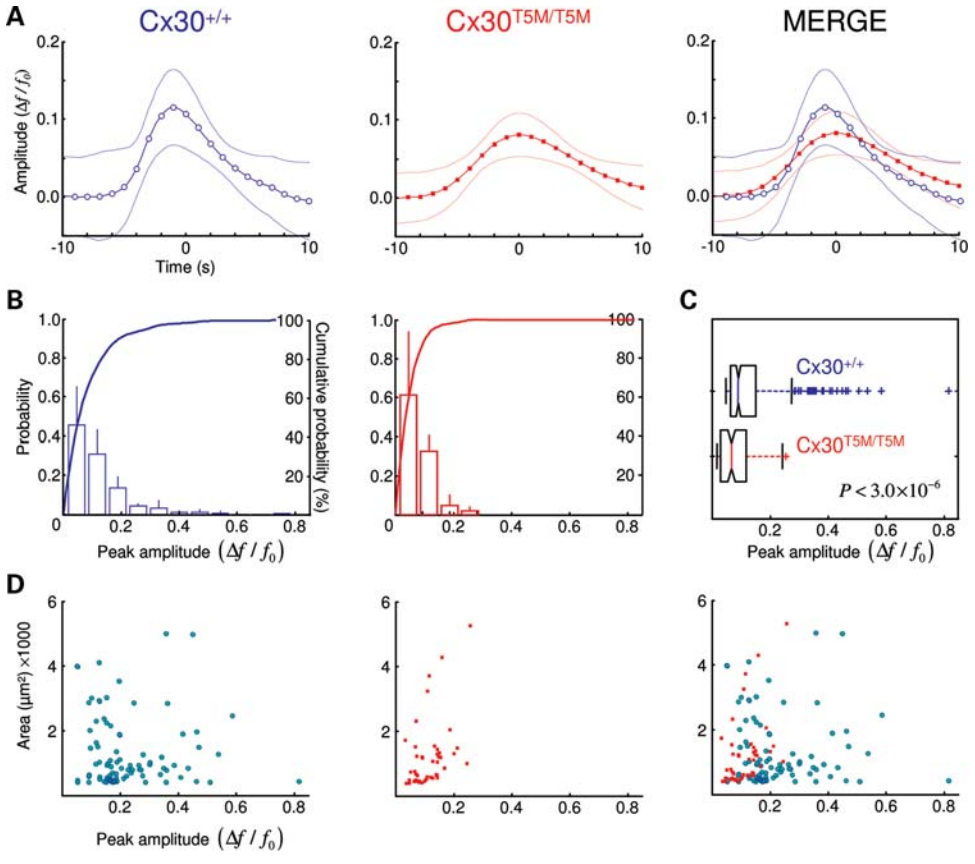

Figure 7. Significantly reduced spontaneous Ca^{2+} signalling activity in the developing cochlea of $Cx30^{T5M/T5M}$ mice. Pooled data obtained by recording spontaneous Ca^{2+} transients for 7 min in each of $n = 4$ cultures from four different mice of each genotype ($Cx30^{+/+}$, $Cx30^{+/T5M}$, $Cx30^{T5M/T5M}$). (**A**) Waveforms of spontaneous Ca^{2+} transients versus time; solid lines are spline interpolations through average data (symbols) and dashed lines mark 95% confidence intervals. (**B**) Probability histograms of Ca^{2+} transient peak amplitude. Error bars represent s.d.; solid lines are peak amplitude cumulative probability. (**C**) Box-and-whisker diagrams for data in (B). For symbolism, see http://en.wikipedia.org/wiki/File:Boxplot_vs_PDF.png. $P < 3 \times 10^{-6}$ indicates the probability that the means of $Cx30^{+/+}$ and $Cx30^{T5M/T5M}$ data are equal based on one-way ANOVA. (**D**) Scatter plots of area invaded by Ca^{2+} transients versus peak amplitude.

development stage (50) was $12.6 \pm 0.6\ \mu m^2$ (mean ± s.e.m., $n = 48$ cells). Thus, on average, a single event involved the spreading of Ca^{2+} signals within ~100 cells of either genotype. However, both frequency of occurrence and the peak amplitude of the Ca^{2+} transients were significantly reduced in $Cx30^{T5M/T5M}$ cultures, compared with $Cx30^{+/+}$ controls, by a factor of 3.6 and 2.0, respectively (Table 1). In accord with this result, the number of distinct ATP release sites and the number of events in $Cx30^{+/+}$ cultures exceeded those of $Cx30^{T5M/T5M}$ cultures by a factor of ~2 and ~4, respectively. Time-dependent waveforms of spontaneous Ca^{2+} transient transients were, on average, smaller and broader in $Cx30^{T5M/T5M}$ cultures than in the corresponding $Cx30^{+/+}$ controls (Fig. 7A). The distributions of amplitudes overlapped at small values, whereas medium- to large-amplitude events were missing altogether in $Cx30^{T5M/T5M}$ cultures (Fig. 7B and C).

Table 1. Properties of spontaneous events

	$Cx30^{+/+}$	$Cx30^{T5M/T5M}$	*P*-value
Peak amplitude ($\Delta f/f_0$)	0.22 ± 0.14	0.11 ± 0.05	$<3 \times 10^{-6}$
Events/min	14.0 ± 5.9	3.9 ± 1.3	<0.015

Data are mean ± s.d. for independently repeated experiments on cultures from $n = 4$ different animals of each type. *P*-value indicates the probability that the means of $Cx30^{+/+}$, and $Cx30^{T5M/T5M}$ data are equal based on one-way ANOVA.

DISCUSSION

In the present study, we generated and characterized a mouse line that expresses the human dominant-negative Cx30T5M mutation under the control of the endogenous Cx30 promoter after homologous recombination in mouse embryonic stem cells (Fig. 1). $Cx30^{T5M/T5M}$ mice showed mild hearing impairments with significantly increased hearing thresholds of ~15 dB at all frequencies, whereas $Cx30^{+/T5M}$ mice displayed no significant differences in hearing compared with $Cx30^{+/+}$ mice (Fig. 2A and Supplementary Material, Fig. S2). Corresponding to the mild hearing phenotype, we found normal endocochlear potential (Fig. 2B) and morphology of the inner ear in adult $Cx30^{T5M/T5M}$ mice. In contrast to $Cx30^{-/-}$ mice, in which Cx30 expression is ubiquitously abrogated (19), the Cx30T5M

protein was still expressed in adult $Cx30^{T5M/T5M}$ mice (Fig. 3 and Supplementary Material, Figs S3 and S4), although we observed a reduction by about one-third in comparison to wild-type Cx30 levels (Fig. 4A). We also detected a significant down-regulation of Cx26 in adult $Cx30^{T5M/T5M}$ mice (Fig. 4B). However, the residual Cx26 and Cx30 proteins are clearly sufficient to maintain the normal endocochlear potential measured in Cx30T5M mice (Fig. 2B). Electrical coupling between non-sensory cells of the developing cochlea, probed by dual patch-clamp recordings, was similar in cochlear organotypic cultures from $Cx30^{+/+}$ and $Cx30^{T5M/T5M}$ mice, in accord with the results obtained in transfected HEK293 cells overexpressing the mutant Cx30T5M protein (22). However, the transfer of the fluorescent tracer calcein was reduced in Cx30T5M mice (Fig. 5), as was intercellular Ca^{2+} signalling due to spontaneous ATP release from connexin hemichannels (Figs 6 and 7).

Other authors hypothesize that heteromeric Cx26/Cx30 channels are essential for normal auditory function (3,51). It is well described that Cx26 and Cx30 are co-localized in most cochlear gap junction plaques where they form heteromeric channels (3,51). Intercellular Ca^{2+} transfer was observed to be faster through overexpressed heteromeric channels than in the corresponding homomeric channels (51). Furthermore, heteromeric Cx26/Cx30 channels in transfected HeLa cells exhibited altered permeability properties compared with their homomeric counterparts: Cx26 homotypic gap junction channels transferred both anionic and cationic tracers, whereas Cx30 homotypic channels showed a restricted permeability to cationic tracers (3). Heteromeric Cx26/Cx30 channels thereby showed permeability properties lying in-between both homotypic channels. Thus, heteromeric channels were permeable to both cationic and anionic tracers. The anionic tracer calcein could pass through heteromeric Cx26/Cx30 and homotypic Cx26 channels, but not through homotypic Cx30 channels. This indicates that Cx26 can support the passage of molecules, which otherwise would not pass through Cx30 homotypic channels. As mentioned above, permeability to calcein was reduced in the developing cochlea of $Cx30^{T5M/T5M}$ mice, whereas electrical coupling, and therefore also permeability to K^+, was unaffected. We conclude that the mutated heteromeric channels could account for the reduction of calcein transfer in these cells.

Earlier studies support this conclusion (22,27). Thus, work performed in expression systems revealed that Cx30T5M protein traffics to the cell membrane where it forms gap junction channels (in accord with our immunofluorescence data in cochlear preparations; Fig. 3 and Supplementary Material, Figs S3 and S4), showing an impaired permeability to neurobiotin (27), propidium iodide and IP_3 (22) (in accord with our fluorescence recovery after photobleaching and Ca^{2+} imaging data; Figs 5–7), whereas permeability to small ions was not affected by the Cx30T5M channels (22) (in accord with our dual patch-clamp recordings in cochlear organotypic cultures).

Similar to human patients suffering from the Cx30T5M mutation, transgenic Cx30T5M mice reveal no obvious skin abnormalities (data not shown). However, human carriers of the Cx30T5M mutation with non-syndromic hearing impairment show increased thresholds between 20 and 50 dB at frequencies of 2–8 kHz and profound sensorineural deafness (21). Compared with human patients, it is surprising that Cx30T5M mice display such a mild hearing phenotype. The differences in severity between mice and humans might be tentatively attributed to differences in the expression or permeability of human versus murine connexin channels. Thus, human Cx26 (hCx26), hCx30 and mouse Cx26 (mCx26) were analysed in transfected HeLa cells, which were microinjected with tracers of different sizes and charges and further characterized using the double patch-clamp technique (52). In that study, mCx26 gap junction channels were permeable to all tested tracers up to a molecular mass of 622 Da (calcein). Compared with its murine counterpart, hCx26 channels showed a higher efficiency in dye transfer and permitted the transfer of larger tracer molecules (Alexa Fluor 594, 759 Da).

Currently, two different hypotheses to elucidate the function of connexins in the inner ear are controversially discussed. On the one hand, impaired K^+-transfer (13,53) could lead to deafness, and on the other hand, impaired biochemical coupling could be the cause of deafness linked to connexin mutations (23). However, it is noteworthy that deafness and lack of endocochlear potential in $Cx30^{-/-}$ mice correlated with developmental disruption of the endothelial barrier of the capillaries supplying the stria vascularis, significant down-regulation of betaine homocysteine S-methyltransferase, restricted to the stria vascularis, and local increase in homocysteine, a known factor of endothelial dysfunction (29), without a clearly identified link to the channel function of connexins. The mild hearing phenotype of $Cx30^{T5M/T5M}$ mice is unlikely to arise from impaired K^+ recirculation through the network of cochlear gap junctions, as our data indicate that electrical coupling is normal in the developing cochlea of homozygous $Cx30^{T5M/T5M}$ mice. Instead, according to the recently published structural analyses of the Cx26 gap junction channel, the localization of the mutation may account for an impairment of biochemical coupling, because the molecular cut-off size and charge selectivity of the channel are influenced by the properties of N-terminal amino acid residues (7). The substitution of the threonine by a methionine residue in Cx30T5M mice might therefore account for impaired biochemical coupling in cochlear non-sensory cells. Our findings support the notion that impaired biochemical coupling can cause defective hearing in mice and man (23). A key role might be played, at the developmental level, by spontaneous Ca^{2+} signalling activity (Fig. 6) (42,43), which is significantly decreased in cochlear cultures from P5 $Cx30^{T5M/T5M}$ mice compared with $Cx30^{+/+}$ controls (Fig. 7 and Table 1).

MATERIALS AND METHODS

Cloning of the Cx30T5M targeting vector

The human Cx30T5M mutation (21) was inserted by PCR mutagenesis in the wild-type mouse Cx30, cloned into the pBluescript vector and sequenced in both directions by AGOWA (Berlin, Germany). The reporter gene was inserted as an nls-LacZ into the pBluescript_Cx30T5M vector by *Bam*HI digestion. An IRES cassette (Clontech Laboratories, CA, USA) was inserted between both coding DNAs via

*Cla*I/*Nsi*I digestion. The construct contained two homologous regions, which flanked the Cx30T5M-IRES-nls-LacZ construct: a 4797 bp 5′ upstream fragment and 1244 bp downstream fragment of Cx30 genomic DNA. For the selection in embryonic stem cells, the neomycin resistance cassette and its promoter DNA, flanked by frt-sites, were cloned downstream of the LacZ reporter cDNA sequence by *Sal*I digestion. The functionality of the frt-sites was analysed by transformation into Flp recombinase expressing *Escherichia coli* bacteria (54). The final targeting vector was characterized by restriction site analyses and afterwards partially sequenced.

Screening of embryonic stem cell clones for homologous recombination

For transfection of murine embryonic stem cells (HM1) (55) by electroporation (800 V, 3 μF), 150 μg of *Xho*I linearized targeting vector DNA was used. Cells containing the vector were selected using 350 mg/ml of G418 (Invitrogen, Karlsruhe, Germany) and analysed by PCR using a upstream primer binding in the LacZ gene of the targeting vector (Cx30_Neo_for: 5′-CCA TCT TGT TCA ATG GCC GAT C-3′) and an external downstream primer specific for the Cx30 3′ region (Cx30_rev: 5′-CCA GAG ACT TGT GGC ACA CTG TG-3′). The PCR-positive clones were additionally characterized by Southern blot hybridization. For this purpose, genomic DNA was extracted and digested with *Bam*HI (5′ external probe), *Hpa*I (3′ external probe) and *Eco*RI (internal probe). After separation on agarose gels, blotting onto Hybond N+ membranes (Amersham Biosciences, Buck, UK) and ultraviolet crosslinking for fixation, hybridization was performed under stringent conditions using the Quick Hyb solution (Stratagene, La Jolla, CA, USA) at 68°C for 2 h. A 766 bp fragment of the 5′ region served as the external probe, a 806 bp fragment of the 3′ region as the 3′ external probe and a 630 bp fragment of the Cx30 coding sequence served as the internal probe.

Generation and genotyping of the Cx30T5M mice

Homologously recombined embryonic stem cell clones were injected into C57BL/6 blastocysts, as described previously (56). The resulting chimeras were mated with C57BL/6 mice. Germline transmission of the recombinant allele in agouti offspring was confirmed by the PCR analysis of isolated tail DNA. Heterozygous Cx30T5M mice were backcrossed with C57BL/6 mice to increase the C57BL/6 genetic background. For all experiments, littermates of >87.5% C57BL/6 genetic background were used. Genotyping was performed by PCR analysis using two 5′ upstream primers, the first binds directly behind the lacZ reporter coding DNA (GenCx30_for: 5′-CTT CAG CTC CAG TGT ACA C-3′) and the second one binds in the neomycin resistance coding DNA (GenNeo: 5′-CTA TCG CCT TCT TGA CGA G-3′), and one 3′ downstream primer which binds in the 3′ homologous region (GenCx30_rev: 5′-CAC CTT AAG AGC ACA CAC TAG CTC-3′). The following PCR protocol was used: 94°C for 5 min, 35 cycles of 94°C for 30 s, 60°C for 45 s and 72° for 1 min, giving rise to a 630 bp fragment of the wild-type allele, a 825 bp fragment of the recombined allele and a 784 bp fragment after deletion of the neomycin cassette.

The T5M mutation was detected by PCR analysis using the primers Cx30_for (5′-GTC AAT TAA TGG CAT TGT TTC ACC-3′ and Cx30_rev (5′-CGG GAT CCA TGC ATC AGA TCA ATG TTG TCT ACA AAG AGG-3′) followed by a digestion with the restriction enzyme *Sph*I. PCR conditions were: 5 min at 94°C, 35 cycles of 30 c at 94°C, 1 min at 60°C, 1 min at 72°C, followed by 10 min at 72°C. After completing the PCR 5 μl of 'buffer 2' and 1 μl of *Sph*I (New England Biolabs, Ipswich, USA) were added and the complete mix was incubated for at 37°C 3 h. The PCR product was demonstrated as a 1436 bp amplicon, and the presence of the mutation was proven by four additional bands at 1184, 594, 590 and 252 bp.

The genotypes were further characterized by Southern blot hybridization. For this purpose, genomic DNA was extracted and digested with *Bam*HI. After separation on agarose gels, blotting onto Hybond N+ membranes (Amersham Biosciences) and ultraviolet crosslinking for fixation, hybridization was performed under stringent conditions using the Quick Hyb solution (Stratagene) at 68°C for 2 h. A 600 bp fragment of the 5′ region was used as the probe.

Quantification of connexin expression by western blot analysis

Total cochlear proteins were extracted from 10 P30 cochleae in 1× Complete (Roche, Mannheim, Germany) and subsequently sonificated three times for 15 s during incubation on ice. Samples were centrifuged at 16 000 g for 10 min (4°C). Laemmli buffer (57) was added to the supernatants. Proteins (100 μg) were separated by electrophoresis on 12% sodium dodecyl sulphate–polyacrylamide gel and transferred to a Hybond ECL membrane (Amersham Biosciences). After blocking with 5% milk powder in washing buffer (8.5 mM Tris–HCl, 1.7 mM Tris–base, 50 mM NaCl, 0.1% Tween-20) for 1 h at room temperature, the membrane was incubated overnight at 4°C with mouse Cx26 (dilution factor 1:500; Invitrogen, Paisley, UK, Cat. No. 13-8100) or rabbit Cx30 antibodies (dilution factor 1:500; Invitrogen, Cat. No. 71-2200). The membrane was washed with washing buffer three times at room temperature before and after 45 min incubation with goat anti-mouse or goat anti-rabbit horseradish peroxidase-conjugated antibodies (dilution factor 1:10 000; Dianova, Hamburg, Germany). Finally, the membranes were incubated with enhanced chemiluminescence reagents (Pierce, Rockford, IL, USA) and developed on X-ray films (Super RX, FUJIFILM Europe, Düsseldorf, Germany). The concentration of the loaded proteins was analysed by immunoblot of β-actin protein (dilution factor 1:500; Sigma, Munich, Germany, Cat. No. A-4700) Connexin protein expression was quantified using the Herolab E.A.S.Y Win32 quantification software (Herolab GmbH, Wiesloch, Germany).

In vivo recordings of endocochlear potential and auditory brainstem responses

These recordings were performed in mice of the following genotypes: $Cx30^{+/+}$, $Cx30^{+/T5M}$, $Cx30^{T5M/T5M}$ and $Cx30^{-/-}$,

aged between P18 and P90. All animal studies were approved by the University of Padua guidelines for animal care and housing or authorized by the UK Home Office.

To measure endocochlear potential, mice were anaesthetized with 0.01 ml/g body weight of 20% urethane, a tracheal cannula was inserted and the bulla opened to reveal the cochlea while the body temperature was kept at 38°C by a feedback-controlled heating pad. A small hole was made in the bony wall of the cochlea over the basal turn scala media, and a micropipette electrode filled with 150 mM KCl was advanced through the hole and through the spiral ligament of the lateral wall into the scala media. The potential difference between the scala media and a reference silver/silver chloride pellet under the dorsal skin was recorded (58).

To record auditory brainstem responses, mice were anaesthetized with an intraperitoneal injection of zolazepam (25 μg/g) and xylazine (10 μg/g). Supplemental doses were then administered as needed while the body temperature was kept at 38°C by a feedback-controlled heating pad. Each recording procedure lasted up to 70 min. Acoustic stimuli were produced in the free field within a foam-padded, shielded acoustic chamber by a System 3 Real-time Signal Processing System combined with an ES1 electrostatic speaker (Tucker-Davis Technologies, Alachua, FL, USA) positioned 4 cm lateral to the left ear of the mouse (59). Stimuli were calibrated by means of an ECM8000 measurement microphone (Behringer International GmbH, Willich, Germany), mounted on the 800B Larson-Davis sound level meter and placed in the position to be occupied by the mouse ear. Stimuli consisted of tone bursts (1 ms rise/decay; 3 ms plateau) at 8, 14, 20, 26 and 32 kHz, and clicks (0.1 ms) delivered at a repetition rate of 13 Hz. A maximum peak equivalent sound pressure level (SPL) of 100 dB (re: 20 μPa) was employed for clicks as well as tone bursts. Decreasing SPLs of 10 dB were employed, starting from a maximum of 100 dB SPL. To minimize contralateral acoustic stimulation, the outer ear canal of the right ear was filled with condensation-vulcanizing silicone mixed with hardener paste (Otoform A flex, in double cartridges; Dreve Otoplastik, Unna, Germany) delivered through a mixing canulas (diameter 5.4 mm) and dispensed by an injector (DS50; Dreve Otoplastik). Acquisition and analysis time was 12 ms for each single stimulus. Responses were recorded between subcutaneous needle electrodes inserted at the vertex (active), ventrolateral to the left ear (reference) and above the tail (ground). Potential differences were amplified (50 000×) with an isolated instrumentation amplifier, band-pass-filtered below 100 Hz and above 8000 Hz and digitized at a rate of 40 000 samples per second. Response waveforms were typically obtained from averages of 400 stimuli presented at the rate of 13 per second for each stimulus condition, saved in the non-volatile memory of a computer and finally displayed on a computer screen.

Analysis of auditory brainstem responses

LabWIEW software (version 8.0.1; National Instruments, Austin, TX, USA) was used for measurements and analysis of amplitude and latency of auditory brainstem responses. To reduce noise and abrupt transitions in the temporal domain, traces were smoothed digitally by low-pass finite-impulse response filtering with equi-ripple characteristics using the Parks–McClellan algorithm. Low-pass frequency was fixed two octaves below the original sampling frequency. For quality control, the smoothed trace was checked against the original trace on the computer display. Wave amplitudes were calculated by a peak detection algorithm as the difference between the two values represented by response maxima (peak) and minima (valley). The algorithm fitted a quadratic polynomial curve to sequential groups of data points (the number of data points used in the fit was 3). Peak latencies were determined relative to the onset of the acoustic stimulus. Wave IV was the most stable and robust evoked response at all intensity levels and for all types of stimulus. The corresponding peak was therefore utilized to estimate auditory brainstem response threshold, defined as the lowest SPL at which any peak could be detected above the residual noise by an experimentally experienced observer blind with respect to genotype. If no wave was detected at maximum intensity stimulation, a nominal threshold of 110 dB SPL was assigned. If any wave was detected at the minimum intensity stimulation of 1 or 10 dB SPL, a nominal threshold of the same level was assigned. Stimuli of lower intensities were not applied due to intrinsic limitations of the sound delivery system.

Reagents and drugs for fluorescence imaging

Membrane permeable AM ester derivatives of fluo-4 and calcein were obtained from Invitrogen/Molecular Probes (Milan, Italy). Carbenoxolone (CBX), pluronic F-127 and sulphinpyrazone were purchased from Sigma (Milan, Italy).

Preparation of cochlear organotypic cultures

Cochleae were dissected from P5 mouse pups in ice-cold HEPES-buffered (10 mM, pH 7.2) Hanks' balanced salt solutions (Sigma, Milan) and placed onto glass cover slips coated with 136 μg/ml of Cell Tak (Becton Dickinson, Milan, Italy). Cultures were incubated in Dulbecco's modified Eagle's medium/F12 (Invitrogen, Leek, The Netherlands), supplemented with FBS 5% and maintained at 37°C for 1 day.

Preparation of cochlear transversal sections for immunofluorescence

Cochleae were dissected from P30 mice, fixed in 4% paraformaldehyde and decalcified overnight in ethylenediaminetetraacetic acid (0.3 M). After three washes in phosphate-buffered saline (PBS), preparations were included in 3% agarose dissolved in PBS and cut perpendicularly to the modiolar axis in 100 μm thickness steps using a vibratome (VT 1000S; Leica Mikrosysteme Vertrieb GmbH, Wetzlar, Germany) set at speed 6 and frequency 6 (both on a scale of 10) and equipped with double-edge razor blades (Platinum, Gillette).

Immunohistochemistry and confocal imaging

Tissues were fixed in 4% paraformaldehyde for 20 min at room temperature and rinsed in PBS containing 2% bovine serum albumin (rinse solution). Cultures were permeabilized

for 1 h at room temperature with 0.1% Triton X-100, dissolved in the rinse solution, whereas transverse slices were permeabilized for 3 h. In both preparations, Cx26 or Cx30 were immunolabelled by overnight incubation at 4°C with specific polyclonal rabbit antibodies anti-Cx26 (Invitrogen, Leek, Cat. No. 51-2800) and anti Cx30 (Invitrogen, Cat. No. 71-2200) diluted in the rinse solution (2.5 μg/ml). Primary antibodies were omitted in negative controls. Cultures were then washed three times in PBS (5 min each time), whereas transverse slices were washed for 1 h each time. For cultures, secondary antibodies (Alexa Fluor® 488 goat anti-rabbit IgG, Invitrogen, Cat. No. A-11008) were applied at 5 μg/ml for 1 h at room temperature, while F-Actin was stained by incubation with Texas red-X phalloidin (Invitrogen, Cat. No. T7471) and nuclei were stained with 4′,6-diamidino-2-phenylindole, dihydrochloride (DAPI; Invitrogen, Cat. No. D1306), both diluted in the rinse solution (1:200). For transverse slices, incubation periods were extended to overnight. After washing for further three times in PBS, samples were mounted onto glass slides with a mounting medium (FluorSave™ Reagent; Merk, Cat. No. 345789) and analysed using a confocal microscope (TCS SP5; Leica) equipped with an oil-immersion objective (either 40× HCX PL APO 1.25 N.A. or 63× HCX PL APO 1.4 N.A.; Leica). Alexa Fluor® 488 was excited by the 488 nm line of an air-cooled argon-ion laser (225 mW, Series 800; National Laser Company, UT, USA) and its fluorescence emission was recorded in a spectral window between 495 and 540 nm. Texas red was excited by the 561 nm line of a diode-pumped solid-state laser (10 mW, Model YLK 6110T, LasNova 60 yellow series 60; LASOS Lasertechnik GmbH, Jena, Germany) and its emission was collected between 600 and 690 nm. DAPI was excited by the 405 nm line of a diode laser module (50 mW, Radius 405-50; Coherent Inc., CA, USA) and its emission was collected between 410 and 440 nm. Laser line intensities and detector gains were carefully adjusted to minimize spectral bleed-through artifacts.

Calcein measurements and fluorescence recovery after photobleaching

Focal irradiation of live cochlear cultures was used to photobleach calcein, as described previously (2,25,26). Calcein is a polyanionic fluorescein derivative that exhibits fluorescence essentially independent of pH between 6.5 and 12. It has about six negative and two positive charges at pH 7 (net charge −4, MW 622) and permeates through gap junction channels in the immature organ of Corti (25). In these experiments, the output of a TTL-controlled semiconductor lased module (or 50 mW, 405 nm, part number LGT 405-60, LG-Laser Technologies GmbH, Kleinostheim, Germany) was injected into a UV-permissive fibre-optic cable (single mode 0.1 N.A., mode field diameter 3.2 ± 0.5 μm, part number P1-405A-FC-2; Thorlabs GmbH, Dachau, Germany); fibre output was collected through a collimating aspheric lens (5 mm effective focal length, part number HPUCO-23A-S-6.2AS; LG-Laser Technologies GmbH), and the re-collimated beam was directed onto a dichromatic mirror (440 dclp; Chroma Technology Corp., Bellows Falls, VT, USA) placed at 45° just above the objective lens of the microscope. By carefully adjusting the position of the fibre in front of the aspheric lens with a two-axis micromanipulator (part number HPT1, Thorlabs), we projected a sharp image of the illuminated fibre core (spot) onto the specimen focal plane selected by the (infinity corrected) objective lens. Under these conditions, the fibre-optic diameter determined accurately the laser-irradiated area, which encompassed one to few cells, depending on cell size and location within the sensory epithelium (26).

For staining with calcein, live cultures were incubated for 10 min at 37°C in and EXM (containing 138 mM NaCl, 5 mM KCl, 2 mM $CaCl_2$, 0.3 mM NaH_2PO_4, 0.4 mM KH_2PO_4, 10 mM HEPES-NaOH and 6 mM D-glucose, pH 7.2, 320 mOsm) supplemented with 5 μM calcein-AM, plus 250 μM sulphinpyrazone and 0.01 w/v pluronic F-127 to prevent dye sequestration and secretion (60). For recording, cultures were transferred on the stage of an upright fluorescence microscope (BX51; Olympus Corporation, Tokio, Japan) and perfused in an EXM for 20 min at 2 ml/min to allow for de-esterification, and thereafter maintained in still EXM at room temperature. Calcein fluorescence was excited and detected using a U-MGFHQ filter cube (Olympus) incorporating a BP460-480 excitation filter, a DM485HQ dichromatic mirror and a BA495-540HQ barrier (emission) filter. Cultures were imaged with a 60× water immersion objective (0.90 NA, Lumplan FL; Olympus) and fluorescence emission was monitored with a cooled charge-coupled device (CCD) camera (Sensicam QE, PCO AG, Kelheim, Germany). In all experiments, the effects of photobleaching due to sample illumination in the 460–480 nm spectral window were kept under control by carefully selecting the most appropriate inter-frame interval (4 s) while controlling light exposure (50 ms) with a mechanical shutter triggered by the frame-valid (FVAL) signal of the CCD camera. Baseline fluorescence in the 495–540 nm emission window was recorded for 2 min, followed by focal laser irradiation at 405 nm to bleach intracellular calcein. Laser irradiation intervals were adjusted to cause 50% photobleaching of the mean baseline fluorescence, which required 0.5 s for tall columnar cells of the greater epithelial ridge and 1.2 s for non-sensory cell of the lesser epithelial ridge (Fig. 5A). Fluorescence recovery after photobleaching was monitored for up to 10 min. Image sequences were acquired using software developed in the laboratory, stored on disk and processed off-line using the Matlab 7.0 software package (The MathWorks, Inc., Natick, MA, USA).

For the analysis of fluorescence recovery after photobleaching, we delineated a region of interest (ROI) inside the bleached (b) area, plus an ROI in a proximal unbleached (u) area, and we computed the ratios of fluorescence intensities (f_b/f_u) at each time point, as described in Ortolano *et al*. (2) Anselmi *et al.* (25) and Majumder *et al*. (26).

Dual patch-clamp recordings

Non-sensory cells in cochlear organotypic cultures bathed in EXM were also probed by dual patch-clamp recordings, as described previously (6,23,52,61–63). Glass capillaries for patch-clamp recordings were formed on a vertical puller (PP-83; Narishige, Tokyo, Japan) from 1.5 mm outer diameter

soda glass (Harvard Apparatus, Edenbridge, UK) and filled with an intracellular solution containing (in mM): 140 CsCl, 2 BAPTA, 10 TEA, 1 $CaCl_2$, 10 HEPES (pH adjusted to 7.2 with KOH). Current and voltage were low-pass-filtered (8 pole Bessel filter, 3 kHz corner frequency) and sampled at 20 kHz using a Digidata 1322A interface (Molecular Devices, Sunnyvale, CA, USA) and pClamp9 software (Molecular Devices). To measure junctional conductance, each cell of an adjacent pair was voltage-clamped independently with one of two Axoclamp 200B amplifiers (Molecular Devices) and kept at the same holding potential ($V_h = -90$ mV), close to the resting membrane potential. By stepping the voltage in one cell (cell 1) while keeping the potential of cell 2 at V_h, thus establishing a transient transjunctional voltage $V_j \equiv V_1 - V_2 = \Delta V_1$, junctional current ($I_j$) was measured directly as the current change in the unstepped cell (i.e. $I_j = -\Delta I_2$). Values of junctional conductance (g_j) were calculated by dividing I_j/V_j, corrected for the error due to the access resistance of both pipettes.

Ca^{2+} imaging

Cochlear cultures were incubated for 60 min at 37°C in an EXM supplemented with fluo-4 AM (16 μM), pluronic F-127 (0.01%, w/v) and sulphinpyrazone (250 μM). For recording, cultures were transferred to the stage of an upright fluorescence microscope (BX51, Olympus) and perfused in an EXM for 20 min at 2 ml/min to allow for de-esterification. Fluo-4 fluorescence was excited at 470 nm by a fast-switching monochromator (Polychrome V, Till Photonics GmbH, Gräfelfing, Germany) and directed onto the sample through a dichromatic mirror (505 dcxr, Chroma). Fluorescence emission was selected by a band-pass emission filter, centred around the 520 nm wavelength (HQ520/40M filter, Chroma), to form fluorescence images on a scientific-grade CCD camera (SensiCam; PCO AG) using a 20× water immersion objective (NA 0.95, XLumPlan FL, Olympus). To record spontaneous Ca^{2+} transients, the EXM was replaced by an ECM (25), a medium containing a reduced concentration of Ca^{2+} (20 μM) similar to that found in endolymph (64). Image sequences were acquired using software developed in the laboratory, stored on disk and processed off-line using the Matlab 7.0 software package (The MathWorks, Inc., Natick, MA, USA). Signals were measured as relative changes of fluorescence emission intensity ($\Delta f/f_0$), where f_0 is initial (pre-stimulus) fluorescence, f is fluorescence at post-stimulus time t and $\Delta f = f - f_0$ (65).

All patch-clamp and live cell imaging experiments were performed at room temperature (24–26°C).

SUPPLEMENTARY MATERIAL

Supplementary Material is available at *HMG* online.

ACKNOWLEDGEMENTS

We thank Christine Siegmund for her excellent technical assistance in the Bonn laboratory.

Conflict of Interest statement. None declared.

FUNDING

This work was supported by grants to F.M., K.P.S. and K.W. from the European commission under the Sixth Research Frame Program of The European Union (FP6 Integrated Project EuroHear, grant number LSHGCT20054512063), by grants to F.M. from Fondazione Cariparo (Progetti di Eccellenza 2006–2007), Telethon Italy (grant number GGP09137), Italian Ministry of Research (PRIN 2007, grant number 2007BZ4RX3_003), by a grant to K.W. of the German Research Foundation (grant number Wi270/30–1) and by the Wellcome Trust to K.P.S. (grant number 079643). Funding to pay the Open Access publication charges for this article was provided by Comitato Telethon Fondazione ONLUS.

REFERENCES

1. Nickel, R. and Forge, A. (2008) Gap junctions and connexins in the inner ear: their roles in homeostasis and deafness. *Curr. Opin. Otolaryngol. Head Neck Surg.*, **16**, 452–457.
2. Ortolano, S., Di Pasquale, G., Crispino, G., Anselmi, F., Mammano, F. and Chiorini, J.A. (2008) Coordinated control of connexin 26 and connexin 30 at the regulatory and functional level in the inner ear. *Proc. Natl Acad. Sci. USA*, **105**, 18776–18781.
3. Yum, S.W., Zhang, J., Valiunas, V., Kanaporis, G., Brink, P.R., White, T.W. and Scherer, S.S. (2007) Human connexin26 and connexin30 form functional heteromeric and heterotypic channels. *Am. J. Physiol. Cell Physiol.*, **293**, C1032–1048.
4. Kumar, N.M. and Gilula, N.B. (1996) The gap junction communication channel. *Cell*, **84**, 381–388.
5. Harris, A.L. (2007) Connexin channel permeability to cytoplasmic molecules. *Prog. Biophys. Mol. Biol.*, **94**, 120–143.
6. Hernandez, V.H., Bortolozzi, M., Pertegato, V., Beltramello, M., Giarin, M., Zaccolo, M., Pantano, S. and Mammano, F. (2007) Unitary permeability of gap junction channels to second messengers measured by FRET microscopy. *Nat. Methods*, **4**, 353–358.
7. Maeda, S., Nakagawa, S., Suga, M., Yamashita, E., Oshima, A., Fujiyoshi, Y. and Tsukihara, T. (2009) Structure of the connexin 26 gap junction channel at 3.5 A resolution. *Nature*, **458**, 597–602.
8. Cohen-Salmon, M., del Castillo, F.J. and Petit, C. (2005) Connexins responsible for hereditary deafness—the tale unfolds. In Winterhager, E. (ed.), *Gap Junctions in Development and Disease*. Springer-Verlag, Berlin, pp. 111–134.
9. Mikaelian, D., Alford, B.R. and Ruben, R.J. (1965) Cochlear potentials and 8 nerve action potentials in normal and genetically deaf mice. *Ann. Otol. Rhinol. Laryngol.*, **74**, 146–157.
10. Jagger, D.J. and Forge, A. (2006) Compartmentalized and signal-selective gap junctional coupling in the hearing cochlea. *J. Neurosci.*, **26**, 1260–1268.
11. Spicer, S.S. and Schulte, B.A. (1998) Evidence for a medial K+ recycling pathway from inner hair cells. *Hear Res.*, **118**, 1–12.
12. Hibino, H. and Kurachi, Y. (2006) Molecular and physiological bases of the K+ circulation in the mammalian inner ear. *Physiology (Bethesda)*, **21**, 336–345.
13. Zdebik, A.A., Wangemann, P. and Jentsch, T.J. (2009) Potassium ion movement in the inner ear: insights from genetic disease and mouse models. *Physiology (Bethesda)*, **24**, 307–316.
14. Sadanaga, M. and Morimitsu, T. (1995) Development of endocochlear potential and its negative component in mouse cochlea. *Hear. Res.*, **89**, 155–161.
15. Tasaki, I. and Spyropoulos, C.S. (1959) Stria vascularis as source of endocochlear potential. *J. Neurophysiol.*, **22**, 149–155.
16. Cohen-Salmon, M., Ott, T., Michel, V., Hardelin, J.P., Perfettini, I., Eybalin, M., Wu, T., Marcus, D.C., Wangemann, P., Willecke, K. *et al.* (2002) Targeted ablation of connexin26 in the inner ear epithelial gap

junction network causes hearing impairment and cell death. *Curr. Biol.*, **12**, 1106–1111.
17. Kudo, T., Kure, S., Ikeda, K., Xia, A.P., Katori, Y., Suzuki, M., Kojima, K., Ichinohe, A., Suzuki, Y., Aoki, Y. *et al.* (2003) Transgenic expression of a dominant-negative connexin26 causes degeneration of the organ of Corti and non-syndromic deafness. *Hum. Mol. Genet.*, **12**, 995–1004.
18. Sun, Y., Tang, W., Chang, Q., Wang, Y., Kong, W. and Lin, X. (2009) Connexin30 null and conditional connexin26 null mice display distinct pattern and time course of cellular degeneration in the cochlea. *J. Comp. Neurol.*, **516**, 569–579.
19. Teubner, B., Michel, V., Pesch, J., Lautermann, J., Cohen-Salmon, M., Sohl, G., Jahnke, K., Winterhager, E., Herberhold, C., Hardelin, J.P. *et al.* (2003) Connexin30 (Gjb6)-deficiency causes severe hearing impairment and lack of endocochlear potential. *Hum. Mol. Genet.*, **12**, 13–21.
20. Ahmad, S., Tang, W., Chang, Q., Qu, Y., Hibshman, J., Li, Y., Sohl, G., Willecke, K., Chen, P. and Lin, X. (2007) Restoration of connexin26 protein level in the cochlea completely rescues hearing in a mouse model of human connexin30-linked deafness. *Proc. Natl Acad. Sci. USA*, **104**, 1337–1341.
21. Grifa, A., Wagner, C.A., D'Ambrosio, L., Melchionda, S., Bernardi, F., Lopez-Bigas, N., Rabionet, R., Arbones, M., Monica, M.D., Estivill, X. *et al.* (1999) Mutations in GJB6 cause nonsyndromic autosomal dominant deafness at DFNA3 locus. *Nat. Genet.*, **23**, 16–18.
22. Zhang, Y., Tang, W., Ahmad, S., Sipp, J.A., Chen, P. and Lin, X. (2005) Gap junction-mediated intercellular biochemical coupling in cochlear supporting cells is required for normal cochlear functions. *Proc. Natl Acad. Sci. USA*, **102**, 15201–15206.
23. Beltramello, M., Piazza, V., Bukauskas, F.F., Pozzan, T. and Mammano, F. (2005) Impaired permeability to Ins(1,4,5)P3 in a mutant connexin underlies recessive hereditary deafness. *Nat. Cell Biol.*, **7**, 63–69.
24. Piazza, V., Ciubotaru, C.D., Gale, J.E. and Mammano, F. (2007) Purinergic signalling and intercellular Ca^{2+} wave propagation in the organ of Corti. *Cell Calcium*, **41**, 77–86.
25. Anselmi, F., Hernandez, V.H., Crispino, G., Seydel, A., Ortolano, S., Roper, S.D., Kessaris, N., Richardson, W., Rickheit, G., Filippov, M.A. *et al.* (2008) ATP release through connexin hemichannels and gap junction transfer of second messengers propagate Ca^{2+} signals across the inner ear. *Proc. Natl Acad. Sci. USA*, **105**, 18770–18775.
26. Majumder, P., Crispino, G., Rodriguez, L., Ciubotaru, C.D., Anselmi, F., Piazza, V., Bortolozzi, M. and Mammano, F. (2010) ATP-mediated cell-cell signaling in the organ of Corti: the role of connexin channels. *Purinergic Signal.*, **6**, 167–187.
27. Common, J.E., Becker, D., Di, W.L., Leigh, I.M., O'Toole, E.A. and Kelsell, D.P. (2002) Functional studies of human skin disease- and deafness-associated connexin 30 mutations. *Biochem. Biophys. Res. Commun.*, **298**, 651–656.
28. Rodriguez, C.I., Buchholz, F., Galloway, J., Sequerra, R., Kasper, J., Ayala, R., Stewart, A.F. and Dymecki, S.M. (2000) High-efficiency deleter mice show that FLPe is an alternative to Cre-loxP. *Nat. Genet.*, **25**, 139–140.
29. Cohen-Salmon, M., Regnault, B., Cayet, N., Caille, D., Demuth, K., Hardelin, J.P., Janel, N., Meda, P. and Petit, C. (2007) Connexin30 deficiency causes instrastrial fluid-blood barrier disruption within the cochlear stria vascularis. *Proc. Natl Acad. Sci. USA*, **104**, 6229–6234.
30. Levin, M. (2007) Gap junctional communication in morphogenesis. *Prog. Biophys. Mol. Biol.*, **94**, 186–206.
31. Wade, M.H., Trosko, J.E. and Schindler, M. (1986) A fluorescence photobleaching assay of gap junction-mediated communication between human cells. *Science*, **232**, 525–528.
32. Eggston, A.A. and Wolff, D. (1947) Embryology of the ear. In *Histopathology of the Ear, Nose, and Throat*. Williams and Wilkins Co., Baltimore, pp. 37–64.
33. Lim, D. and Rueda, J. (1992) Structural development of the cochlea. In Romand, R. (ed.), *Development of Auditory and Vestibular Systems 2*. Elsevier, Amsterdam, pp. 33–58.
34. Bermingham-McDonogh, O., Oesterle, E.C., Stone, J.S., Hume, C.R., Huynh, H.M. and Hayashi, T. (2006) Expression of Prox1 during mouse cochlear development. *J. Comp. Neurol.*, **496**, 172–186.
35. Rabut, G. and Ellenberg, J. (2005) Photobleaching techniques to study mobility and molecular dynamics of proteins in live cells: FRAP, iFRAP, and FLIP. In Goldman, R.D. and Spector, D.L. (eds), *Live Cell Imaging*. Cold Spring Harbor Laboratory, New York, pp. 101–126.
36. Rozental, R., Miduturu, S. and Spray, D.C. (2001) How to close a gap junction channel. In Bruzzone, R. and Giaume, C. (eds), *Connexin Methods and Protocols*. Humana Press, Totowa, NJ, pp. 447–476.
37. Zhao, H.B., Yu, N. and Fleming, C.R. (2005) Gap junctional hemichannel-mediated ATP release and hearing controls in the inner ear. *Proc. Natl Acad. Sci. USA*, **102**, 18724–18729.
38. Valiunas, V. and Weingart, R. (2000) Electrical properties of gap junction hemichannels identified in transfected HeLa cells. *Pflugers Arch.*, **440**, 366–379.
39. Muller, D.J., Hand, G.M., Engel, A. and Sosinsky, G.E. (2002) Conformational changes in surface structures of isolated connexin 26 gap junctions. *EMBO J.*, **21**, 3598–3607.
40. Bennett, M.V., Contreras, J.E., Bukauskas, F.F. and Saez, J.C. (2003) New roles for astrocytes: gap junction hemichannels have something to communicate. *Trends Neurosci.*, **26**, 610–617.
41. Goodenough, D.A. and Paul, D.L. (2003) Beyond the gap: functions of unpaired connexon channels. *Nat. Rev. Mol. Cell Biol.*, **4**, 285–294.
42. Tritsch, N.X., Yi, E., Gale, J.E., Glowatzki, E. and Bergles, D.E. (2007) The origin of spontaneous activity in the developing auditory system. *Nature*, **450**, 50–55.
43. Tritsch, N.X. and Bergles, D.E. (2010) Developmental regulation of spontaneous activity in the mammalian cochlea. *J. Neurosci.*, **30**, 1539–1550.
44. Zhang, Y., McBride, D.W. Jr and Hamill, O.P. (1998) The ion selectivity of a membrane conductance inactivated by extracellular calcium in *Xenopus* oocytes. *J. Physiol.*, **508**, 763–776.
45. Stout, C.E., Costantin, J.L., Naus, C.C. and Charles, A.C. (2002) Intercellular calcium signaling in astrocytes via ATP release through connexin hemichannels. *J. Biol. Chem.*, **277**, 10482–10488.
46. Eskandari, S., Zampighi, G.A., Leung, D.W., Wright, E.M. and Loo, D.D. (2002) Inhibition of gap junction hemichannels by chloride channel blockers. *J. Membr. Biol.*, **185**, 93–102.
47. Bruzzone, R., Barbe, M.T., Jakob, N.J. and Monyer, H. (2005) Pharmacological properties of homomeric and heteromeric pannexin hemichannels expressed in *Xenopus* oocytes. *J. Neurochem.*, **92**, 1033–1043.
48. Gomes, P., Srinivas, S.P., Van Driessche, W., Vereecke, J. and Himpens, B. (2005) ATP release through connexin hemichannels in corneal endothelial cells. *Invest. Ophthalmol. Vis. Sci.*, **46**, 1208–1218.
49. Retamal, M.A., Froger, N., Palacios-Prado, N., Ezan, P., Saez, P.J., Saez, J.C. and Giaume, C. (2007) Cx43 hemichannels and gap junction channels in astrocytes are regulated oppositely by proinflammatory cytokines released from activated microglia. *J. Neurosci.*, **27**, 13781–13792.
50. Hinojosa, R. (1977) A note on development of Corti's organ. *Acta Otolaryngol.*, **84**, 238–251.
51. Sun, J., Ahmad, S., Chen, S., Tang, W., Zhang, Y., Chen, P. and Lin, X. (2005) Cochlear gap junctions coassembled from Cx26 and 30 show faster intercellular Ca^{2+} signaling than homomeric counterparts. *Am. J. Physiol. Cell Physiol.*, **288**, C613–623.
52. Beltramello, M., Bicego, M., Piazza, V., Ciubotaru, C.D., Mammano, F. and D'Andrea, P. (2003) Permeability and gating properties of human connexins 26 and 30 expressed in HeLa cells. *Biochem. Biophys. Res. Commun.*, **305**, 1024–1033.
53. Kikuchi, T., Adams, J.C., Miyabe, Y., So, E. and Kobayashi, T. (2000) Potassium ion recycling pathway via gap junction systems in the mammalian cochlea and its interruption in hereditary nonsyndromic deafness. *Med. Electron Microsc.*, **33**, 51–56.
54. Buchholz, F., Angrand, P.O. and Stewart, A.F. (1996) A simple assay to determine the functionality of Cre or FLP recombination targets in genomic manipulation constructs. *Nucleic Acids Res.*, **24**, 3118–3119.
55. Magin, T.M., McWhir, J. and Melton, D.W. (1992) A new mouse embryonic stem cell line with good germ line contribution and gene targeting frequency. *Nucleic Acids Res.*, **20**, 3795–3796.
56. Theis, M., Magin, T.M., Plum, A. and Willecke, K. (2000) General or cell type-specific deletion and replacement of connexin-coding DNA in the mouse. *Methods*, **20**, 205–218.
57. Laemmli, U.K. (1970) Cleavage of structural proteins during the assembly of the head of bacteriophage T4. *Nature*, **227**, 680–685.
58. Steel, K.P. and Barkway, C. (1989) Another role for melanocytes: their importance for normal stria vascularis development in the mammalian inner ear. *Development*, **107**, 453–463.

59. Santarelli, R., Arslan, E., Carraro, L., Conti, G., Capello, M. and Plourde, G. (2003) Effects of isoflurane on the auditory brainstem responses and middle latency responses of rats. *Acta Otolaryngol.*, **123**, 176–181.
60. Di Virgilio, F., Steinberg, T.H. and Silverstein, S.C. (1989) Organic-anion transport inhibitors to facilitate measurement of cytosolic free Ca^{2+} with fura-2. *Methods Cell Biol.*, **31**, 453–462.
61. Lagostena, L., Ashmore, J.F., Kachar, B. and Mammano, F. (2001) Purinergic control of intercellular communication between Hensen's cells of the guinea-pig cochlea. *J. Physiol.*, **531**, 693–706.
62. Lagostena, L., Cicuttin, A., Inda, J., Kachar, B. and Mammano, F. (2001) Frequency dependence of electrical coupling in Deiters' cells of the guinea pig cochlea. *Cell Commun. Adhes.*, **8**, 393–399.
63. Bicego, M., Beltramello, M., Melchionda, S., Carella, M., Piazza, V., Zelante, L., Bukauskas, F.F., Arslan, E., Cama, E., Pantano, S. *et al.* (2006) Pathogenetic role of the deafness-related M34T mutation of Cx26. *Hum. Mol. Genet.*, **15**, 2569–2587.
64. Bosher, S.K. and Warren, R.L. (1978) Very low calcium content of cochlear endolymph, an extracellular fluid. *Nature*, **273**, 377–378.
65. Mammano, F. and Bortolozzi, M. (2010) Ca2+ imaging: principles of analysis and enhancement. In Verkhratsky, A. and Petersen, O. (eds), *Calcium Measurement Methods*. Humana Press, New York, Vol. 43, pp. 57–80.